ACS Sustainable Chemistry & Engineering

pubs.acs.org/journal/ascecg

Research Article

Structure and Dynamic Properties of a Glycerol–Betaine Deep Eutectic Solvent: When Does a DES Become an Aqueous Solution?

Hugo Monteiro, Alexandre Paiva, Ana Rita C. Duarte, and Nuno Galamba*

Cite This: *ACS Sustainable Chem. Eng.* 2022, 10, 3501–3512

Read Online

ACCESS | Metrics & More | Article Recommendations | Supporting Information

ABSTRACT: Deep eutectic solvents (DESs) are an emerging class of green solvents with a wide spectrum of potential applications whose properties may be further tailored through the addition of water. Here, we study, through molecular dynamics, the influence of water on the properties of a betaine–glycerol–water (B:G:W) DES (1:2:ζ; ζ = 0 to 100), aiming at getting insight into the structural and dynamic crossover between a DES and an aqueous solution. The density, shear viscosity, and diffusion coefficients are found to exhibit a non-linear dependence of ζ, similar to that observed for the solvation layers' composition. Each Gly and Bet are replaced, respectively, by ∼3 and ∼5 water molecules, with the highest rates of depletion being found for Gly around Bet and Gly around Gly. Above ζ = 7 (70 mol %; 29.5 wt %), a major structural transformation occurs, with the complete disruption of the second Bet-Gly solvation layer and the formation of a new second layer at a shorter distance, accompanied by a sudden change in the rate of increase of the components' diffusion. Nonetheless, opposite to other DES, our results indicate a smooth crossover between a DES and an aqueous solution.

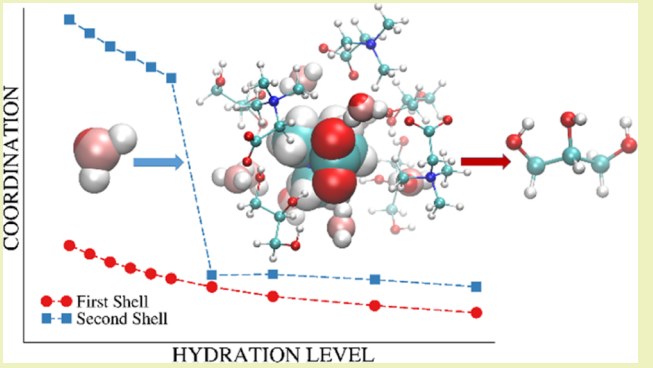

KEYWORDS: *green solvents, viscosity, diffusion, structure, molecular dynamics*

1. INTRODUCTION

Deep eutectic solvents (DESs) are a relatively novel[1] class of solvents, normally liquid at room temperature, characterized by a depression of the melting point, relative to its components, at the eutectic composition.[2,3] Many DESs share some of the general characteristics of ionic liquids (ILs), such as low vapor pressure and high thermal stability, although exhibiting, in general, several advantages[2] such as ease of preparation, reduced cost, and biodegradability.

Besides the abovementioned properties, the main interest in DESs stems from the wide scope of potential applications[2,4] of these systems, ranging from extraction and separation processes[5,6] to (bio)catalysis[7,8] or CO_2 capture.[9,10] DESs can be formed by mixing two or more components that can be salts, natural compounds[11] (NADES), or therapeutic components[12] (THEDES) and are classified into different categories (Type I to V), with mixtures formed by a quaternary ammonium salt and a hydrogen bond donor (Type III) being the most studied.[2,3]

In the past years, many experimental,[13−21] theoretical,[18,22−24] and simulation[24−29] studies have addressed the distinct properties of DESs. Nonetheless, the molecular mechanisms that govern the structure–property relationships in this class of solvents remain poorly understood.[2] Thus, while the melting point depression is closely linked with the hydrogen bond (HB) network formed between the components, a comprehensive picture of the relationship between structure, molecular interactions, and the properties of the DES remains elusive. Furthermore, the presence of water, either as a component to form a DES or to tailor properties such as the viscosity, raised several questions about these solvents:[29−43] is there a water ratio at which a transition from a binary to a ternary (where water is the third component) DES occurs? Is there a well-defined crossover between a DES and an aqueous solution? How are water-induced structural transformations related to the solvents' properties?

Hammond et al.[33] studied the water effect on the nanostructure of a series of choline chloride/urea/water (aka reline) DESs through neutron diffraction experiments aided by the empirical potential structure refinement method. The DES nanostructure was retained up to 42 wt % H_2O because of water sequestration around choline cations. At 51 wt % H_2O, the DES structure was disrupted and water–water and DES–

Received: November 3, 2021
Revised: December 27, 2021
Published: March 8, 2022

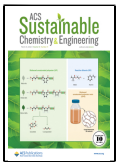

water interactions became dominant, with the mixture being best described as an aqueous solution of the DES components. A structural picture was put forward where a "Water-in-DES" to a "DES-in-Water" transition occurs at 51 wt % (83 mol %) H_2O, based on a discontinuity in the choline−choline and choline−water coordination number.

Sapir and Harries[39] reached similar conclusions in a simulation study, providing evidence of a transition between a "Water-in-DES" (up to ∼30 wt % H_2O) and a "DES-in-Water" (30−50 wt % H_2O) solution for reline, whereas beyond ∼50 wt % H_2O, the solution was best described as an aqueous electrolyte-like mixture.

Ferreira et al.[31] reported the effect of water on the structure and dynamics of a (1:2) choline chloride:glycerol DES through NMR spectroscopy. Three distinct regimes were identified: up to 11 wt % H_2O, where the structure of the DES remains intact, between 11 and 35 wt %, where the DES structure persists, in spite of some solvation of the components, and at 35 wt %, where the structure is disrupted and a transition to an aqueous solution occurs.

Kaur et al.[34] observed, through molecular dynamics, the initiation of the disruption of the structure of choline chloride/ethylene glycol (aka ethaline) at 40 mol % of water, with additional dilution leading to a rapid disruption of the intermolecular interactions between the pure ethaline components.

Understanding the relationship between these water-induced structural transformations and the solvent's properties is critical for the design of optimized solvents for specific applications. Thus, while water addition may favor some applications, by lowering the viscosity, it may hinder others (e.g., gas capture) depending on the water content.[9] Herein, we studied the NADES system glycine betaine−glycerol−water (B:G:W) at various water ratios (1:2:ζ; ζ = 0 to 100), through molecular dynamics simulations, aimed at getting insight into the relationship between the physicochemical properties and the water-induced structural transformations of the DES. Various glycine betaine-based ILs[44,45] and DES[15,46−48] have been reported in the literature. Glycine betaine, hereinafter referred to simply as betaine (Bet), is a solid, decomposing at high temperatures (∼570 K). Instead, glycerol (Gly) is a liquid at room temperature (melting point, T_m = 291 K) and has been widely studied in connection with its glass-forming and cryoprotectant characteristics.[49] While glycerol has been commonly used as a HB donor to form DES,[50] these fall outside a stricter DES definition where both components are solid at room temperature. This specific definition, however, need not concern us here, and emphasis is placed, instead, on the crossover between an aqueous DES and an aqueous solution of the components, namely, whether a specific water fraction exists, below which some definition of a DES persists and above which an aqueous solution can be defined. More importantly, we seek to understand whether such transition translates into a structure−property singularity. The remainder of the article is organized as follows: Section 2 provides a detailed description of the methods and force fields used; Section 3 discusses the results obtained in this study for the binding energies, density, and transport properties; these are then analyzed in the light of the water-induced structural transformations of the DES; and we end with some conclusions in Section 4.

2. METHODS

2.1. Binding Energies. Møller−Plesset second-order perturbation theory[51] (MP2) calculations were performed for all possible dimers comprising the molecules in the aqueous DES, aimed to get insight on the magnitude of the binding energies, ΔE. For this purpose, binding energies, $\Delta E = E_{XY} - (E_X + E_Y)$, were computed by optimizing the geometries of the dimers, XY, and respective monomers (X and Y) in the gas phase at the MP2/aug-cc-pvdz[52] theoretical level. The vibrational zero-point energies (ZPE) were also determined using the analytical harmonic frequencies to calculate $\Delta E_0 = \Delta E + \Delta(\mathrm{ZPE})$. The calculations were performed with the program GAUSSIAN 09.[53] Although no thorough exploration of the potential energy surface was pursued, the reported minima are likely to be either the global minima or low energy local minima, depicting HBs between every possible proton donor−acceptor pair.

2.2. Molecular Dynamics. Molecular dynamics (MD) of a betaine−glycerol (B:G) DES in the ratio (1:2) were carried out for 128 molecules of betaine (Bet) and 256 molecules of glycerol (Gly). The DES−water mixtures were studied for distinct water contents, ζ, namely, B:G:W(1:2:ζ) with ζ = 1, 2, 3, 4, 5, 7, 10, 15, 20, which correspond to the following water molar percentages (mol %) 25, 40, 50, 57, 62.5, 70, 76.9, 83, 87 and weight percentages (wt %) 5.6, 10.7, 15.2, 19.3, 23.0, 29.5, 37.4, 47.3, 54.4. An additional mixture was studied, namely, B:G:W (1:2:100) (97.1 mol %; 85.7 wt %), to probe the structure of the DES in a highly diluted environment where Gly and Bet should be almost completely hydrated. MD of pure glycerol and "supercooled" betaine were also carried out for 256 molecules; notice the latter are only for comparison purposes since the force field for Bet was not validated for the pure solid or liquid (see below).

The MD simulations were carried out in the isothermal−isobaric (NpT) ensemble at 298 K and 0.1 MPa in a cubic box with periodic boundary conditions, with the program GROMACS.[54] The systems were first equilibrated in the NpT ensemble for 5 ns after a 100 ps simulation in the canonical (NVT) ensemble. The trajectories were then propagated in the NpT ensemble for times ranging between 100 ns and 1 μs for the different ζ. Long simulations (1 μs) were required to assess the shear viscosity with a reasonable accuracy for the neat DES (B:G; ζ = 0). The properties reported here for each DES were averaged over three simulations, starting from different initial velocities.

The T and p were controlled with the thermostat of Bussi et al.[55] and the Parrinello−Rahman barostat,[56] and the equations of motion were solved with the Verlet leap-frog algorithm with a 2 1 fs time-step. Electrostatic interactions were computed via the particle-mesh Ewald (PME) method.[57] A cut-off of 1 nm was used for non-bonded van der Waals and for the PME real space electrostatic interactions. Heavy atom-hydrogen covalent bonds were constrained with the LINCS algorithm.[58]

2.3. Force Field. Various force fields were first probed for pure glycerol, namely, GAFF,[59] OPLS-aa,[60] OPLS-aa with 1.14*CM1A-LBCC[61] charges calculated with LigParGen,[62] and OPLS-aa with RESP[63] charges computed at the HF/6-31G* theoretical level (see Figure S1 and Table S1). The density, self-diffusion coefficient, and the shear viscosity of glycerol were assessed for every model. The GAFF model predicted a density of ∼1.30 g·cm^{-3}, compared with the experimental value, 1.26 g·cm^{-3}, and a self-diffusion coefficient lower than the experimental value by an order of magnitude; thus, MD with GAFF were not further pursued. Table S2 summarizes the above properties for the distinct OPLS-aa models. From these, we chose to adopt the OPLS-aa model (see Table S1). Next, we investigated various OPLS-aa models for betaine (see Table S3). The bond stretching, angle bending, and torsional parameters, as well as the Lennard-Jones 12−6 parameters, were obtained from LigParGen[62] and are derived from glycine and tertiary amine models. Since betaine is solid, we assessed the properties of the DES B:G (1:2), at 298 K and 0.1 MPa, namely, the density and the shear viscosity, which have been recently reported in the literature;[46] van der Waals cross interactions were calculated using geometric combination rules. The results are given in Table S4; diffusion coefficients for glycerol and

https://doi.org/10.1021/acssuschemeng.1c07461
ACS Sustainable Chem. Eng. 2022, 10, 3501−3512

betaine are also reported. The most accurate results were obtained with the RESP-HF/6-31G* partial charges, although the viscosity is still largely overpredicted (see Table S4). To improve the FF for betaine, as reflected in the DES properties, we scaled the RESP-HF/6-31G* and the 1.14*CM1A-LBCC[61] charges by a factor $\lambda < 1$, while the remaining parameters were kept unchanged. Notice that the 1.14*CM1A-LBCC charges are already scaled (1.14 scale factor) to account for polarization effects. This scale factor, however, is chosen to minimize the errors of properties such as the density but not viscosity.

We found $\lambda = 0.925$ for RESP-HF/6-31G* to give a reasonable viscosity but a density already too low (see Table S4). The 1.14*CM1A-LBCC charges with $\lambda = 0.85$ in turn provided a better estimate of the density and a viscosity close to the experimental value for the DES at 298 K. Thus, the simulations reported hereinafter were carried out with this latter model for betaine. These results highlight the importance of validating a force field beyond the density. Neglect of the viscosity of the DES would have indicated that the OPLS-aa/1.14*CM1A-LBCC for betaine provided a good description of the DES since a density of 1.204 g·cm^{-3}, closer to the experimental value (~1.218 g·cm^{-3}), is found. However, the viscosity is higher than the experiments by about an order of magnitude. We chose to sacrifice the accuracy of the density (1.185 g·cm^{-3}) in favor of a model that provides a good estimate of the transport properties, specifically, the shear viscosity and possibly the diffusion.

For the study of the aqueous DES with different fractions of water, we used the TIP4P/2005 water model,[64] which provides an excellent description of the structure and dynamics of liquid water.

2.4. Experimental Density. The density of the DES for $\zeta = 20$, for which no close experimental data was available, was measured. The density at $\zeta = 5$ and 10 was also measured allowing to compare with the available experimental data[46] for $\zeta = 5.2$ and 10.2. The measurements were performed with an Anton Paar Stabinger viscometer 3001 from 20 to 60 °C with an increase of 10 °C of temperature per point.

2.5. Transport Coefficients. The diffusion coefficients of the different molecular species in solution were estimated from the mean square displacement (MSD), through the Einstein relation[65]

$$D = \frac{1}{6N}\lim_{t\to\infty}\frac{\mathrm{d}}{\mathrm{d}t}\left\langle \sum_{i=1}^{N} |r_i(t) - r_i(0)|^2 \right\rangle \quad (1)$$

where < > indicates an average over time-origins, $r_i(t)$ and $r_i(0)$ are the positions of the ith particle at time t and at the origin, respectively, and D is the diffusion coefficient, averaged over every particle $i = 1$ to N, for a given molecular species. For normal diffusion, the MSD grows linearly at long times, and D can, thus, be obtained from the slope of the MSD.

The shear viscosity can be calculated through integration of the pressure tensor correlation function[66]

$$\eta = \frac{V}{10k_BT}\int_0^\infty \left\langle \sum_{\alpha\beta}^{9} P_{\alpha\beta}(0)P_{\alpha\beta}(t) \right\rangle \mathrm{d}t \quad (2)$$

where $P_{\alpha\beta}$ is the symmetrized traceless portion of the stress tensor, $\sigma_{\alpha\beta}$, given by[67]

$$P_{\alpha\beta} = \frac{1}{2}(\sigma_{\alpha\beta} + \sigma_{\beta\alpha}) - \frac{1}{3}\delta_{\alpha\beta}\left(\sum_{\alpha}\sigma_{\alpha\alpha}\right) \quad (3)$$

$\sigma_{\alpha\beta}$ is the Kronecker delta and there are six, out of the nine, distinct $P_{\alpha\beta}$ elements. This expression allows improving the statistics over the original Green−Kubo formula which involves the average over only the three different off-diagonal elements, $\sigma_{\alpha\beta} = \sigma_{\beta\alpha}$, of the stress tensor[65]

$$\eta = \frac{V}{3k_BT}\int_0^\infty \left\langle \sum_{\alpha\beta}^{3} \sigma_{\alpha\beta}(0)\sigma_{\alpha\beta}(t) \right\rangle \mathrm{d}t \quad (4)$$

used here for comparison purposes. Despite some differences, consistent values were obtained through eqs 2 and 4 (see Tables S2 and S4).

We note that the viscosity is particularly difficult to calculate accurately because, unlike diffusion, it is a collective property. Furthermore, for highly viscous fluids such as the B:G DES, the stress tensor elements time correlation functions exhibit large fluctuations and converge in a time scale of 10−20 ns at room temperature (see Figure S2). For this reason, 1 μs long trajectories were required to compute η for the B:G DES. For the B:G:W (1:2:ζ) aqueous DES, the viscosity decreases significantly and 0.5 μs long trajectories were enough to estimate the viscosity for $\zeta = 1$, whereas 200 ns trajectories were used for $\zeta = 2$, 3, and 4, and 100 ns for larger ζ.

3. RESULTS AND DISCUSSION

3.1. Binding Energies. Figure 1 displays the optimized geometries of the gas phase dimers formed by glycerol, betaine,

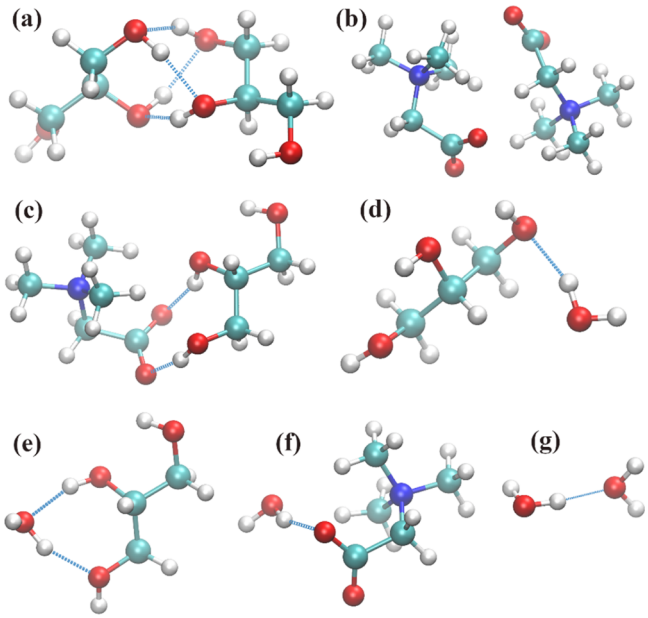

Figure 1. MP2/aug-cc-pvdz-optimized geometries for the gas phase dimers (see Table 1). (a) Glycerol, (b) betaine, (c) glycerol−betaine, (d,e) glycerol−water (single and double HB), (f) betaine-water (single HB; no double HB could be found), and (g) water−water. The blue dashed bonds represent HBs.

and water. The respective binding energies, ΔE, are given in Table 1. The magnitude of ΔE increases in the order: Bet−Bet > Bet−Gly > Gly−Gly > Bet−Wat > Gly-Wat > Wat−Wat, as expected. The high binding energy ($\Delta E = -131$ kJ mol^{-1}) of betaine is associated with strong electrostatic interactions since betaine is a zwitterion. The dipoles of the monomers align in opposite directions (antiparallel) in the dimer. Thus, while the dipole of the monomer is found to be 11.5 D, that of the dimer is only 2.4 D. The large binding energy of the dimer of betaine in the gas phase contrasts with the suggestion that betaine cannot establish strong ion−ion interactions in the liquid due to the shielding of the formal positive charge in the nitrogen by the intramolecular methyl groups.[17] Nonetheless, the magnitude of the binding energies of Bet with the solid phenolic compounds studied in ref 17 could be larger than those for Bet−Bet, unlike for glycerol.

The dimer of glycerol shows four HBs, replaced by two HBs in the betaine−glycerol dimer, between the deprotonated carboxyl group of betaine and the hydroxyl groups of glycerol.

https://doi.org/10.1021/acssuschemeng.1c07461
ACS Sustainable Chem. Eng. 2022, 10, 3501−3512

Table 1. Binding Energies in the Gas Phase without Zero-Point Energy (ZPE) (ΔE) and with ZPE Corrections (ΔE_0) Calculated at the MP2/aug-cc-pvdz Level for the Dimers Involving the Species in the DES[a]

dimer	ΔE (kJ/mol)	ΔE_0 (kJ/mol)
Gly−Gly	−53.7	−44.4
Bet−Bet	−130.5	−122.5
Bet−Gly	−94.6	−86.3
Gly−Wat[d][b]	−31.9	−23.6
Gly−Wat[ad][c]	−39.3	−28.8
Bet−Wat[d][b]	−52.0	−41.0
Wat−Wat	−22.0	−13.2

[a]Basis-set superposition errors were neglected as well as anharmonic effects on the ZPE. [b]d = water HB donor. [c]ad = water HB acceptor and donor.

The latter are strong and the betaine−glycerol ΔE (−95 kJmol^{-1}) is larger by nearly a factor of two relative to the glycerol dimer (−54 kJmol^{-1}). Thus, the Bet−Gly binding energy is similar to the components' average binding energy, $\Delta E_{BG} = (\Delta E_B + \Delta E_G)/2$ since $2\Delta E_{BG} = -189.2$ kJ mol^{-1} and $\Delta E_B + \Delta E_G = -184.2$ kJ mol^{-1}.

Concerning the dimers involving water molecules, again betaine (HB acceptor) forms stronger HBs with water than glycerol (HB acceptor/donor) even when glycerol acts concomitantly as an HB donor and acceptor with a single water molecule (see Figure 1e).

3.2. Density, Shear Viscosity, and Diffusion. Table 2 summarizes the density, shear viscosity, and the diffusion coefficients calculated for pure glycerol, water, and the B:G:W DES for water ratios, ζ, ranging from 0 to 100. The experimental viscosity of glycerol has been reported in a wide range of temperatures.[46,68,69] Segur and Obertar[68] in the 1950's and more recently Schroter and Donth[69] critically evaluated the available data. At 293 K (20 °C), values ranging between 1412 and 1499 mPas were noted by Segur and Obertar.[68] A value of 1323 mPas is found from the Vogel−Fulcher−Tammann (VFT) equation reported by Schroter and Donth in the T range of 283−323 K. A more recent experiment by Rodrigues et al.[46] found a lower viscosity, 1196.4 mPas. Following Schroter and Donth,[69] these discrepancies could be related with the water content in the samples. In the light of these differences, the OPLS-aa force field for glycerol provides a reasonable description of the pure liquid (see Table 2), although lower values are found for the density and diffusion, relative to the experiments; an improved self-diffusion coefficient is found when system size corrections are added.[70,71] With respect to the neat DES, a good agreement is found for the viscosity, while the density is underestimated by 2.5%, with the error decreasing (as expected) with the addition of water.

Table 2 also shows an anticipated slowdown of the water dynamics associated with the formation of Bet−Wat and Gly−Wat HBs and excluded volume effects. The slowdown of the rotational and translational dynamics of water because of volume exclusion results from a retardation of the HB breaking/forming dynamics of water.[72−78] Further dilution[77] increases the number of water neighbors, promoting HB switches and accelerating the rotational and translational dynamics of water.

The density, shear viscosity, and diffusion coefficients of the DES at the different water ratios, ζ, are also plotted in Figure 2, along with the experimental data. The viscosity is in good agreement with the available data, whereas no experimental data could be found for the diffusion coefficients. The viscosity shows a marked decrease with the addition of some water to the system, slowly converging to the viscosity of neat water at high ζ. The diffusion coefficients, however, show an opposite trend slowly increasing up to $\zeta = 7$ and increasing almost linearly for $\zeta \geq 10$.

The density, viscosity, and diffusion coefficient dependence on the water content were found to be well described by the equation

$$Z = Z_0 \exp[-a_z/(\zeta + b_z)] \quad (5)$$

where Z stands for either ρ, η, or D, and Z_0, a_z, and b_z are property-dependent empirical parameters. This equation can be re-written in terms of the water molar fraction x_w in the form

$$Z = Z_0 \exp[-a_z(1 - x_w)/(b_z(x_w - 1) - 3x_w)] \quad (6)$$

Table 2. Density, Viscosity, and Diffusion Coefficients for Pure Glycerol and the DES at 298 K and 0.1 MPa; Note That Water's Diffusion Scale is 3 Decades Larger Than for Glycerol and Betaine

system	ρ^{Exp} (g·cm^{-3})	ρ^{MD} (g·cm^{-3})	η^{Exp} (mPa·s)	η^{MD} (mPa·s)	D_G (10^{-8} cm^2 s^{-1})	D_B (10^{-8} cm^2 s^{-1})	D_W (10^{-5} cm^2 s^{-1})
GLY	1.255[a]	1.246	780[a]; 850[b]	871 ± 78	1.6 ± 0.07[c]		
1:2	1.216[a]	1.185	1528[a]	1536 ± 222	1.0 ± 0.05	0.63 ± 0.05	
1:2:1		1.179		710 ± 18	2.1 ± 0.1	1.4 ± 0.03	0.013
1:2:2		1.173		359 ± 24	4.0 ± 0.1	2.8 ± 0.1	0.022
1:2:3		1.167		177 ± 19	7.1 ± 0.01	4.9 ± 0.1	0.035
1:2:4		1.161		107 ± 6	11.5 ± 0.3	8.5 ± 0.5	0.053
1:2:5	1.173	1.155		72 ± 2	18.5 ± 0.1	13.3 ± 0.1	0.079
1:2:7		1.143		33 ± 3	35.8 ± 1.0	27.0 ± 0.7	0.14
1:2:10	1.140	1.127		15.6 ± 0.2	72.3 ± 1.3	57.4 ± 0.3	0.26
1:2:15		1.106		7.2 ± 0.1	142 ± 3.0	121 ± 4.0	0.47
1:2:20	1.100	1.091		4.1 ± 0.4	207 ± 1.0	186 ± 7.0	0.65
1:2:100		1.026		1.3 ± 0.02	654 ± 3.0	592 ± 7.0	1.69
WAT	0.997	0.997	0.89[d]	0.88 ± 0.05			2.1 ± 0.01[e]

[a]Ref 46. [b]Ref 69; value calculated from the VFT equation fitted to experimental data. [c]The self-diffusion coefficient with system size corrections[70] is 1.8 × 10^{-8} cm^2 s^{-1}. The experimental[79] self-diffusion coefficient of glycerol at 298 K and 0.1 MPa is 2.1 ± 0.3 (10^{-8} cm^2 s^{-1}) (see Table S2). [d]Ref 80. [e]The self-diffusion coefficient with system size corrections[70] is 2.3 × 10^{-5} cm^2 s^{-1}. The experimental[81] self-diffusion coefficient of water at 298 K and 0.1 MPa is 2.3 × 10^{-5} cm^2 s^{-1}.

https://doi.org/10.1021/acssuschemeng.1c07461
ACS Sustainable Chem. Eng. 2022, 10, 3501−3512

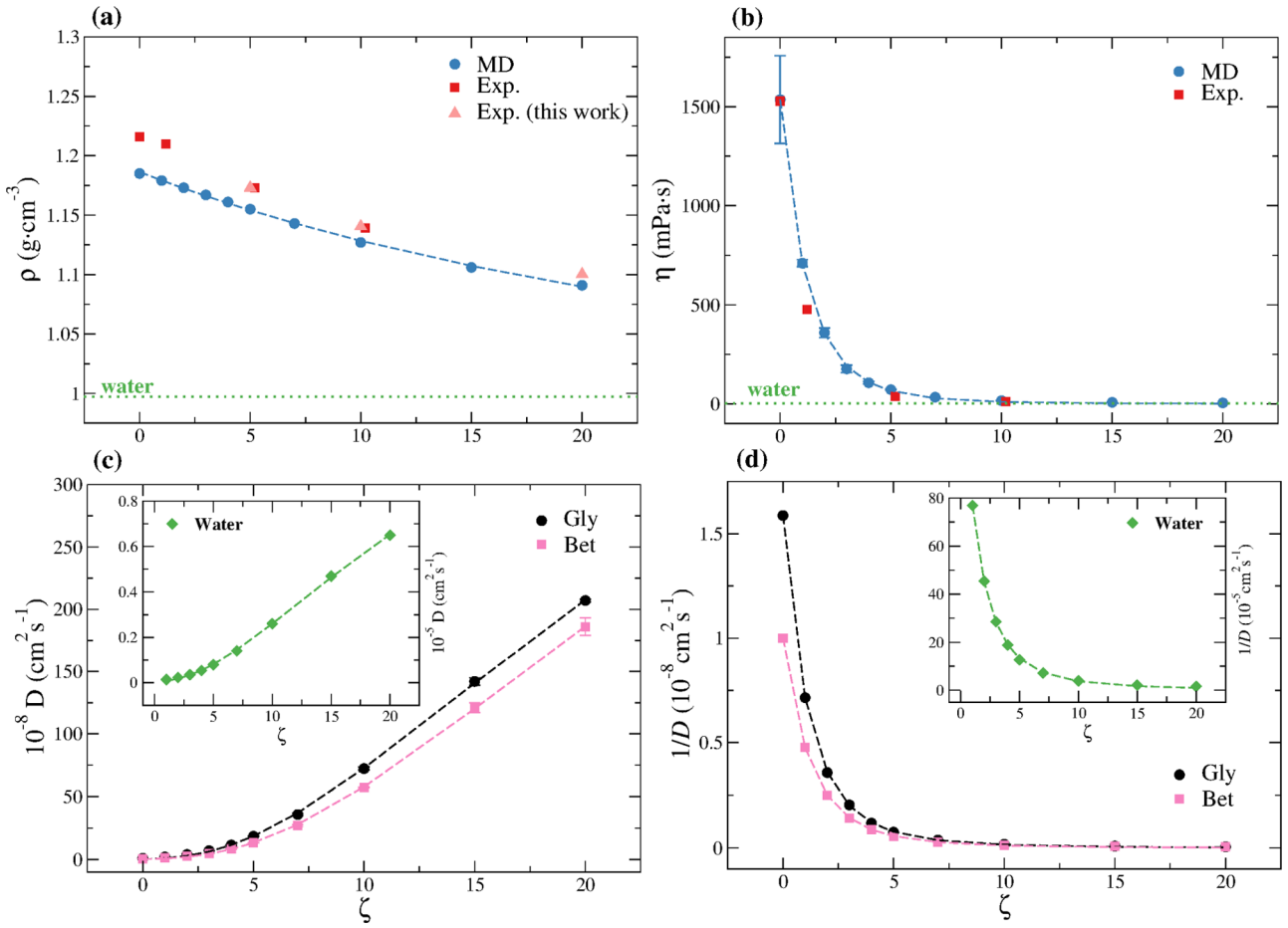

Figure 2. (a) Density (ρ), (b) viscosity (η), (c) diffusion (D), and (d) $1/D$ coefficients at 298 K for the aqueous DES with different water contents, ζ. Results for $\zeta = 100$ are omitted for clarity. The dashed lines are fits to eq 5, with $Z = \rho$, η, D, and $1/D$. The dotted green lines in (a) and (b) are, respectively, the values of the density (0.997 g·cm^{-3}) and viscosity (0.88 m·Pas) of neat water at 298 K and 0.1 MPa.

3.3. Structure and Hydration. We now turn our attention to the structural transformations of the DES, associated with hydration, and the way these relate to the properties of the DES. We assessed the composition of the coordination spheres of Bet, Gly, and water as a function of the water content. To this end, we calculated the radial distribution functions (rdfs) involving the distinct components of the DES, as a function of the water ratio. Unless stated otherwise the reference atoms used to assess the rdfs are the middle C atom of Gly, the N atom of Bet, and the O atom of water, which are close enough to the respective molecular centers of mass. The Bet−Gly (=Gly−Bet), Bet−Bet, and Gly−Gly rdfs are shown in Figure 3. The rdfs exhibit three well-defined peaks (solvation spheres) in the absence of water. The addition of water leads to a progressive loss of the short- and long-range order with the third peak vanishing at $\zeta \sim 5$. A minor shift of the onset and the maximum of the first peak, to longer distances, and of the first minimum to shorter distances can also be seen with the increase of ζ, resulting in a slight contraction of the first layer. This is a direct consequence of hydration, as discussed below. Furthermore, increased mobility of Bet and Gly can be inferred from the increase of the height of the first minimum, reflecting a more frequent crossover between the first and second solvation spheres.

The most prominent feature of Figure 3 is, however, the appearance of a new second peak which for the Bet−Gly rdf occurs for $\zeta > 7$ (Figure 3a); the original second peak is identified by $\zeta = 0$, whereas the new second peak is identified by $\zeta = 100$. As can be seen, the relative height of the latter increases with the decrease of the height of the first peak with ζ. A similar behavior can be observed for the Bet−Bet rdf (Figure 3b) although the onset of the novel second peak appears at a lower water ratio ($\zeta \sim 4$). A more subtle point is the appearance of a new third peak at ∼1.2 nm. Whereas this is also visible in the Bet−Gly rdf, it is more marked for the Bet−Bet function. The Gly−Gly (Figure 3c) rdf also shows a new second peak, although this becomes more noticeable only at $\zeta > 15$ because of a slower decrease of the height of the first peak (i.e., first coordination number). Thus, the new second peaks observed in Figure 3 result from the breakdown of the first coordination sphere into two looser solvation layers where the Bet and Gly molecules are already significantly hydrated and more mobile, which reflects in a higher (and constant) rate of increase of the diffusion coefficients with the water content for $\zeta > 7$ (see Figure 2c).

Concerning the differences between the Gly and Bet coordination in pure Gly and (supercooled) Bet, and in the neat DES ($\zeta = 0$), we find that the Gly−Gly and Bet−Bet coordination numbers (CNs) fall to near 58 and 37%, respectively. Thus, the CN of Gly in the neat liquid is 13.5, whereas in the BG (1:2), CN = 7.8 and that of Bet in the pure supercooled liquid is 13.6 while in the DES, it decreases to 5.0. These numbers reflect the formation of the DES, with Bet and

https://doi.org/10.1021/acssuschemeng.1c07461
ACS Sustainable Chem. Eng. 2022, 10, 3501−3512

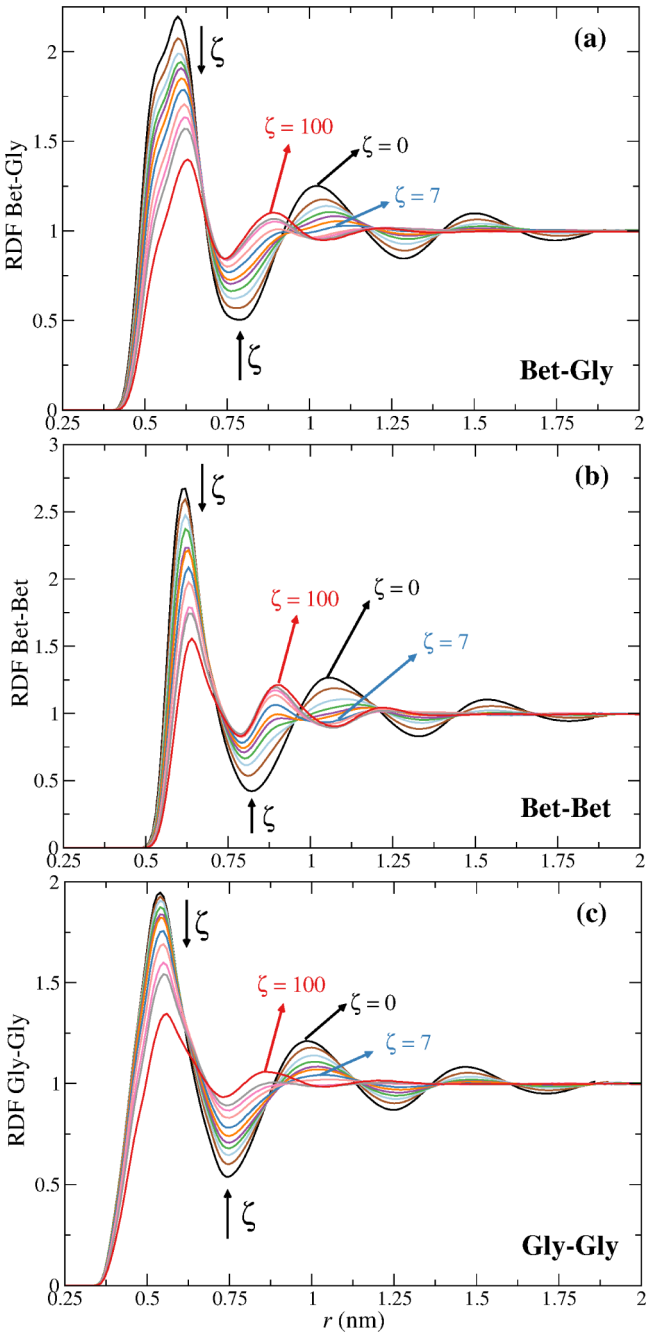

Figure 3. (a) Bet−Gly (same as Gly−Bet), (b) Bet−Bet, and (c) Gly−Gly rdfs at different water compositions. The arrows point toward increasing ζ. The Bet−Gly first CNs = 2 × CNs(Gly−Bet) are 9.7, 8.8, 8.1, 7.5, 6.8, 6.4, 5.6, 4.6, 3.6, 3.0, and 0.8; the Bet−Bet first CNs are 5.0, 4,6, 4.2, 3.9, 3.6, 3.4, 3.0, 2.5, 1.9, 1.6, and 0.4; and the Gly−Gly first CNs are 7.8, 7.5, 7.2, 6.8, 6.5, 6.2, 5.5, 4.8, 3.9, 3.2, and 0.8, corresponding to (ζ = 0, 1, 2, 3, 4, 5, 7, 10, 15, 20, 100).

Gly attaining mixed solvation layers via the formation of Bet−Gly HBs.

Figure 4a shows the variation of the Bet−Gly first and second CNs with ζ. The CNs were computed through the integration of the rdf up to the (variable) first and second minima, accounting for the transformation of the second peak at ζ = 7 (70 mol %; 29.5 wt %). The "CNs" computed for the (fixed) region of the first and second peaks of the neat DES are also depicted (dashed lines), for comparison purposes.

The first CN (i.e., the nearest Gly neighbors of Bet) ranges between 9.7 at ζ = 0 and 3.0 at ζ = 20; at ζ = 100, a value of 0.8 is found. The second CN, in turn, decreases from ∼32 at ζ = 0 to ∼27 at ζ = 5, with a sudden jump to 7 at ζ = 7 and a value of 5.6 at ζ = 20; at ζ = 100, a value of 1.8 is found. If the coordination is assessed at the same spatial region for every ζ, corresponding to the second peak of the neat DES, we find a smoother decrease of the "CN" from ∼32.6 at ζ = 0 to ∼13.8 at ζ = 20.

Figure 4b shows the nearest Gly neighbors of a Bet molecule in the dehydrated DES (ζ = 0) from a MD snapshot. Several Bet molecules can be seen within the inner region of the first solvation sphere, illustrating the fact that Bet−Bet interactions remain important in the DES. However, at ζ = 7, although still in the solvation sphere (Figure 4a), Bet is no longer found in the inner region (see Figure 4c), as a result of hydration.

The depletion/hydration of the Bet and Gly solvation spheres is now analyzed in greater detail. Figure 5 and Table 3 show the CNs for every pair of components of the DES. A relatively steep decrease of the (first) CNs of Bet and Gly, with ζ, can be seen in Figure 5a, especially concerning the depletion of Gly from the Bet's first solvation layer.

Interestingly, the variation of the CNs with ζ is well-described by eq 5, indicating, as expected, a close link between the density, shear viscosity, and diffusion dependence of ζ and the depletion of Gly and Bet from their mutual coordination spheres. The rate of depletion of each component with the water content can be estimated by $dZ/d\zeta$ (Z = CN—see eq 5). Figure 5b shows that the highest rates of depletion occur for Gly from the Bet's coordination sphere, followed by the depletion of Gly around Gly, for $\zeta \geq 2$, with the latter rising above the former for $\zeta \geq 13.5$. The rates of depletion of Bet with ζ, around Gly and Bet, in turn, are similar.

Table 3 shows that each Gly and Bet are replaced, respectively, by ∼3 and ∼5 water molecules. Furthermore, it can be seen that above ζ = 3, there are already more water than glycerol molecules around Bet.

The number of water molecules in the Gly, Bet, and Wat first hydration layers is also displayed in Figure 5c. In contrast with the results of Hammond et al.[33] for reline, we do not observe a discontinuity in the Bet−Wat nor in the Bet−Bet CNs at any water molar fraction. Furthermore, no plateau is found for the Wat−Wat rdf, and the CN of bulk water is not observed even for ζ = 100.

A slightly higher hydration of Bet, compared to Gly, can be seen, suggesting a preferential hydration of Bet. The solvent accessible surface area (SASA) of Bet was found to be 2.92 ± 0.04 nm^2, larger than that of Gly, 2.49 ± 0.04 nm^2, which could explain the above difference; SASAs were computed by rolling a solvent sphere[82,83] of radius 1.4 Å over the van der waals surface[84] of the solutes. However, since the Bet−Gly ratio is 1:2, selective hydration must occur to some extent, with the Bet molecules exhibiting preferential hydration, consistent with gas phase binding energies (Table 1). Thus, although gas phase binding energies lack bulk interactions, this suggests that the HB trends observed in the gas phase also drive the preferential hydration of the components in the liquid. Furthermore, whereas Gly can donate up to 3 protons and accept 3−6 oxygens, Bet can accept a maximum of 4 protons, although the maximum number of HBs is governed by steric effects (see discussion below). A similar preferential hydration was observed for choline relative to urea (and chloride) in reline.[33]

https://doi.org/10.1021/acssuschemeng.1c07461
ACS Sustainable Chem. Eng. 2022, 10, 3501−3512

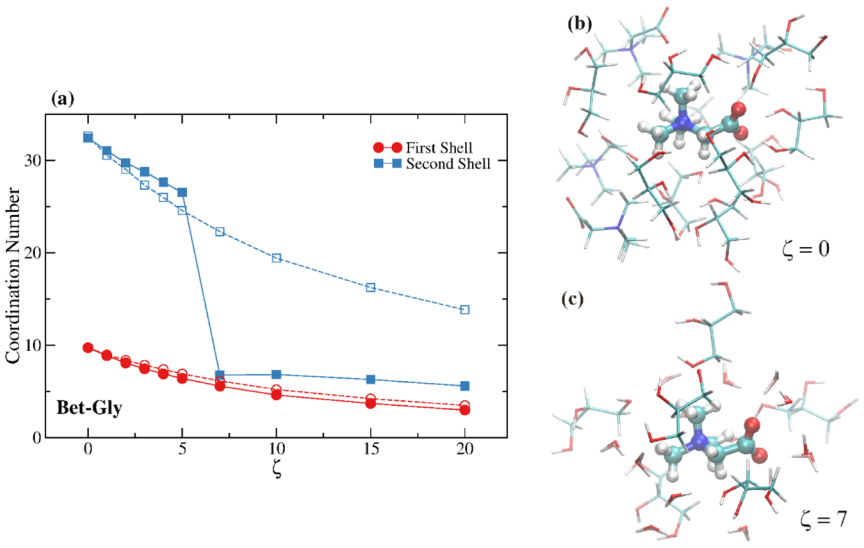

Figure 4. (a) Bet−Gly first and second CNs (filled symbols) obtained through integration of the rdfs' first and second peak, and the "CNs" obtained through integration of the Bet−Gly rdfs first [0−0.785 nm] and second peak [0.785−1.29 nm] for the neat DES (ζ = 0), for every ζ (open symbols). Lines are a guide to the eye. (b,c) MD snapshots showing the nearest neighbors (inner subpopulation of the first coordination sphere) of a molecule of betaine for ζ = 0 and ζ = 7, respectively.

Figure 5c also shows that hydration at ζ = 20 remains much distinct from the hydration in an "infinitely" dilute solution of Bet, showing the persistence of Bet and Gly in their mutual coordination spheres, even at high dilution conditions. Thus, water occupation of Gly and Bet hydration layers and consequent dislodgement of the DES components slowly transforms the DES into an aqueous solution of the components, resulting in a non-linear variation of the properties, seemingly without structure−property discontinuities.

3.4. Hydrogen Bonding and Cavity Occupation. We now discuss the effect of water on the Bet−Gly HBs and the occupation, by water molecules, of cavities in the DES. Figure 6 shows the (Bet)O−HO(Gly) rdfs and the respective CNs for the different water contents. While the rdfs have no HB angular restrictions, the peaks correspond essentially to Bet O···HO Gly HBs formed between Bet (acceptor) and Gly (donor). Figure 6b shows that each O atom of Bet cannot accept more than one proton from glycerol due to steric effects and that, in average, at $\zeta \sim 7$ over 50% of the Bet molecules are no longer hydrogen bonded to Gly. Thus, although the Bet−Gly CN only decreases from 9.7 to 5.6 (see Table 3), many Gly molecules are in the outer region of the solvation layer and do not form HBs with Bet. Again, the CNs' (∼HBs) dependence of ζ is well-described by eq 5.

We now discuss the degree of penetration of water in the DES component solvation spheres and the size of the cavities in the neat DES. Figure 7a,b compares, respectively, the Bet−Gly, Bet−Bet, and Bet−Wat and the Gly−Bet, Gly−Gly, and Gly−Wat rdfs at ζ = 7, illustrating the degree of water penetration within the coordination spheres of Gly and Bet.

As can be seen, because of their small size, water molecules can penetrate deep into the Gly and Bet coordination spheres occupying the cavities in the DES. This occupation weakens the Bet−Gly and Gly−Gly HBs and the ionic interactions between the Bet zwitterions, with water molecules competing with Gly and Bet for the formation of HBs, facilitating, therefore, the displacement of Bet and Gly from their mutual coordination spheres.

To estimate the size of the cavities around Bet in the neat DES, we compared the CNs of Bet−Gly and Bet−Wat in the neat DES (ζ = 0) and the highly diluted DES (ζ = 100), respectively (Figure 7c). This comparison, up to the distance of the onset of the first Bet−Gly peak in the neat DES, allows estimating the number of molecules that fill that cavity, providing a simple estimate of the cavity volume. A similar comparison can be performed for glycerol (Figure 7d). These numbers appear as blue areas in Figure 7c,d corresponding to 1.8 and 1.5 water molecules, respectively. Assuming a water molecule is approximately spherical with a van der Waals radii of 1.4 Å (V = 11.5 Å^3), we find a cavity of ∼21 Å^3 around Bet and ∼17 Å^3 around Gly. Thus, if the neat DES components were frozen and interactions turned off, ∼1.8 and ∼1.5 water molecules could be inserted, in average, around each Bet and Gly, respectively; this corresponds to ζ = 4.8. Figure 7c,d, however, shows that the occupation of such cavities gradually increases with ζ, not reaching a plateau, at least up to ζ = 20. The reason is that turning on the interactions between the DES molecules, including water molecules, results in an increase of the onset of the Bet−Gly, Bet−Bet, and Gly−Gly solvation layers (see Figure 3), favoring water penetration in the above cavities. This in turn results in an acceleration of the HB dynamics favoring the dislodgement of Bet and Gly from their mutual solvation spheres or, similarly, to having Bet and Gly mainly solvated by water molecules.

4. CONCLUSIONS

DES emerged in the past decades as green solvents, aimed at replacing organic solvents and ILs in a plethora of chemical processes and applications. Understanding and modeling the relationship between their composition and properties are key to the development of optimized mixtures for specific applications. The possibility of additional tailoring of the DES' properties through the addition of water raises several important questions concerning the role of water on the solvents' structure and properties. This is especially relevant because whereas water favors some applications (e.g., biocatalytic applications), it may exert the opposite role in

https://doi.org/10.1021/acssuschemeng.1c07461
ACS Sustainable Chem. Eng. 2022, 10, 3501−3512

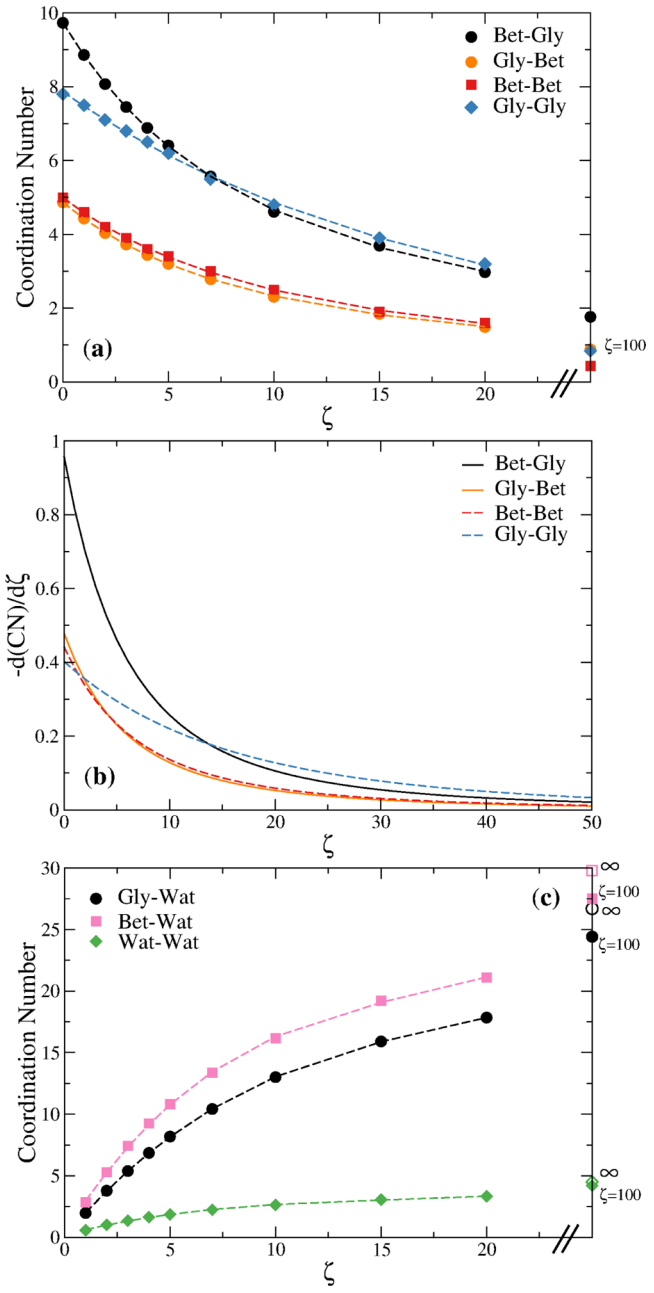

Figure 5. (a) Bet−Gly, Gly−Bet, Bet−Bet, and Gly−Gly CNs for the different DES. The values for $\zeta = 100$ are shown on the rhs of the plot; dashed lines are fits to eq 5 with Z = CN (b) rates of depletion of Gly and Bet from the coordination spheres of Bet and Gly with the water content, as predicted from $dZ/d\zeta$ with Z = CN in eq 5—values were extrapolated up to $\zeta = 50$; (c) X−Wat CNs for the different DES; dashed lines are fits to eq 5. The values for $\zeta = 100$ and for an "infinitely dilute" (∞) solution are shown on the rhs of the plot.

Table 3. First Solvation Sphere CNs for the DES Components for Several Water Ratios (ζ)

	$\zeta = 0$	$\zeta = 1$	$\zeta = 3$	$\zeta = 5$	$\zeta = 7$	$\zeta = 10$	$\zeta = 20$
Bet−Gly	9.7	8.8	7.5	6.4	5.6	4.6	3.0
Bet−Wat		2.9	7.4	10.8	13.4	16.2	21.1
Bet−Bet	5.0	4.6	3.9	3.4	3.0	2.5	1.6
Gly−Bet[a]	4.9	4.4	3.7	3.2	2.8	2.3	1.5
Gly−Wat		2.0	5.4	8.2	10.4	13.0	17.8
Gly−Gly	7.8	7.5	6.8	6.2	5.5	4.8	3.2
Wat−Wat		0.6	1.4	1.9	2.2	2.6	3.3

[a]CN(Gly−Bet) = CN(Bet-Gly)/2.

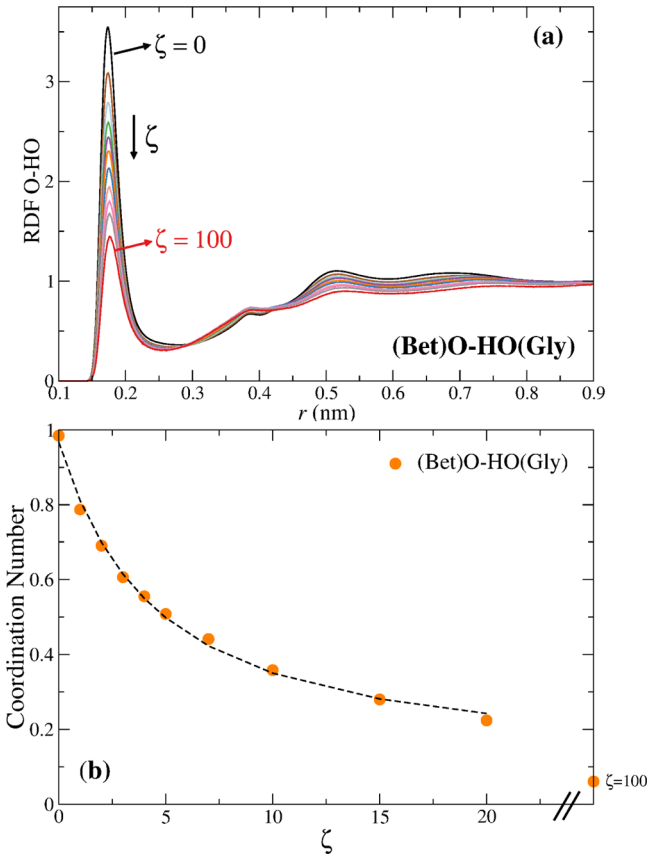

Figure 6. (Betaine)O−HO(Glycerol) (a) rdfs and (b) CNs, at the different ζ values; the dashed line is a fit to eq 5.

others (e.g., greenhouse gas capture). Here, we showed, through molecular dynamics simulations, that a B:G:W DES undergoes a continuous structural transition with the water content, exhibiting a major structural transformation at 70 mol % (29.5 wt %), characterized by the loss of the second Bet−Gly coordination sphere and the emergence of a novel second coordination layer at a shorter distance. This reflects in a larger mobility of the DES components, with a fingerprint on the rate of increase of the diffusion coefficient with the water content. Water molecules are small enough to occupy the cavities near Bet and Gly, weakening the interactions between the DES components, and, therefore, enhancing the diffusion and promoting the dislodgment of the components from their mutual solvation layers. Each Gly and Bet are found to be replaced, respectively, by ∼3 and ∼5 water molecules, and the highest rates of depletion, upon water addition, are observed for Gly around Bet and Gly around Gly. Nevertheless, no major structure−property singularities are found and a smooth transition between a DES and an aqueous solution is observed. This is markedly different from the behavior observed for other DES, in particular, reline,[33] for which a non-continuous structural transformation was found, reflecting a non-monotonic water dependence of the choline−choline and choline−water coordination numbers. Whereas this suggests a major difference between the ability of the choline cation and betaine (zwitterionic) to sequestrate water, the different nature of the HBD (urea and glycerol) could play an important role

https://doi.org/10.1021/acssuschemeng.1c07461
ACS Sustainable Chem. Eng. 2022, 10, 3501−3512

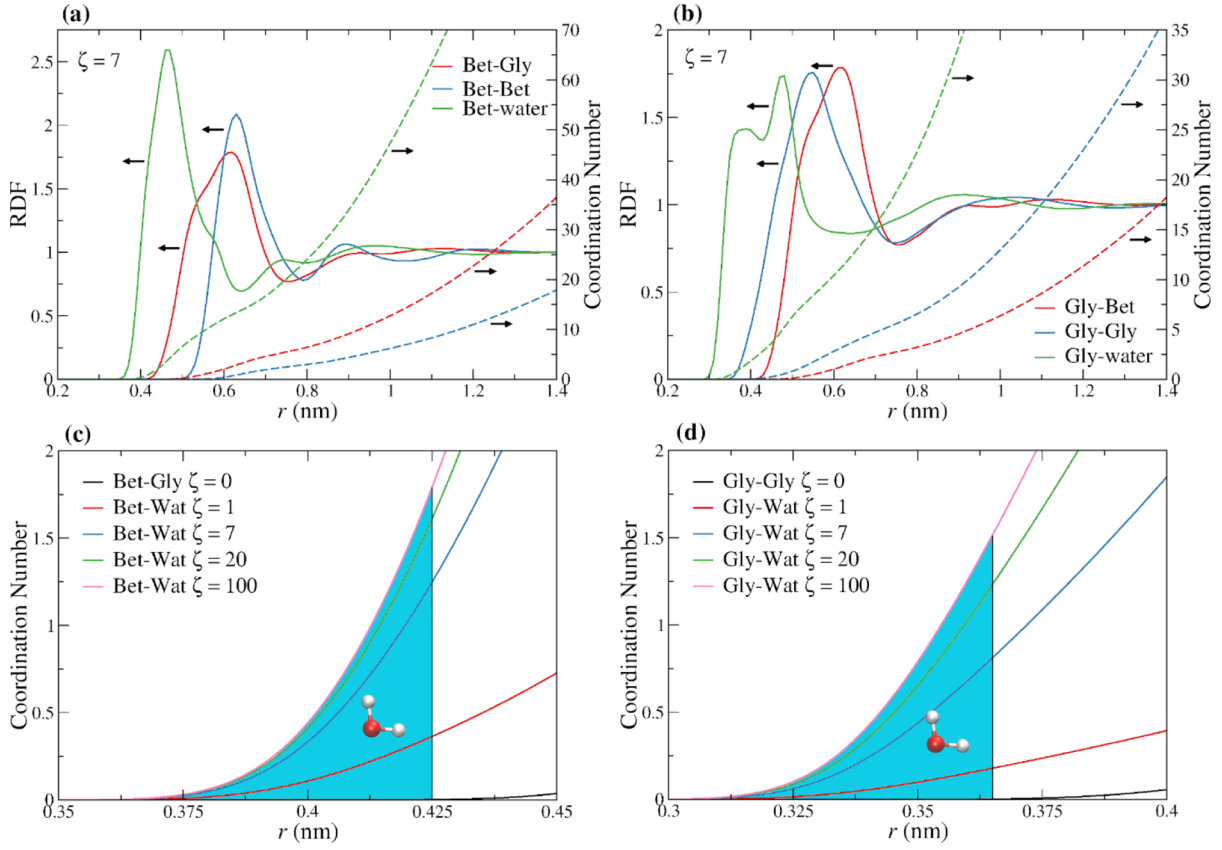

Figure 7. (a) Bet−X (X = Gly, Bet, and water) rdf and respective CN for the B:G:W (1:2:7) DES. (b) Gly−X rdf and respective CN for the B:G:W (1:2:7) DES; the "double" peak for Gly−Wat results from the choice of the middle C atom for Gly; the first peak corresponds to water HBs with the central OH of Gly, whereas the second peak corresponds to water molecules interacting with the end OH groups. The arrows point toward the respective *y*-axis of the curves. (c) Bet−Gly CN in the neat DES and Bet−Wat CNs at different water ratios. The blue region corresponds to the cavity region around Bet occupied by water; the Bet−Gly CN in the neat DES at 0.425 nm is 0.002; the Bet−Wat CN for ζ = 100 is 1.8 water molecules. (d) Gly−Gly CN in the neat DES and Gly−Wat CNs at different water ratios. The blue region corresponds to the cavity region around Gly occupied by water; the Gly−Gly CN in the neat DES at 0.365 nm is 0.002; and the Gly−Wat CN for ζ = 100 is 1.5 water molecules.

concerning the rate of depletion of the HBD around the HBA. This, in turn, should be associated with the magnitude of the HBs formed between the components in the binary mixtures and between the latter and water molecules in the ternary systems. Additional studies will be required to understand the molecular origin of these differences.

■ ASSOCIATED CONTENT

Supporting Information

The Supporting Information is available free of charge at https://pubs.acs.org/doi/10.1021/acssuschemeng.1c07461.

Molecular representation of glycerol and betaine; stress tensor time correlation function and shear viscosity for the pure DES; atomic charges for the glycerol OPLS-aa force field; density, diffusion, and viscosity for glycerol for different atomic partial charges; atomic charges for the betaine OPLS-aa force field; and density, diffusion, and viscosity for the pure DES for different force fields for betaine (PDF)

■ AUTHOR INFORMATION

Corresponding Author

Nuno Galamba − *Biosystems and Integrative Sciences Institute, Faculty of Sciences of the University of Lisbon, 1749-016 Lisbon, Portugal*; orcid.org/0000-0003-1704-2242; Email: njgalamba@fc.ul.pt

Authors

Hugo Monteiro − *LAQV, REQUIMTE, Departamento de Química, Nova School of Science and Technology, 2829-516 Caparica, Portugal*

Alexandre Paiva − *LAQV, REQUIMTE, Departamento de Química, Nova School of Science and Technology, 2829-516 Caparica, Portugal*

Ana Rita C. Duarte − *LAQV, REQUIMTE, Departamento de Química, Nova School of Science and Technology, 2829-516 Caparica, Portugal*

Complete contact information is available at: https://pubs.acs.org/10.1021/acssuschemeng.1c07461

Notes

The authors declare no competing financial interest.

■ ACKNOWLEDGMENTS

A.P. received financial support from FCT through IF/01146/2015. This work has received funding from the ERC-2016-CoG 725034 and was supported by the Associate Laboratory for Green Chemistry (LAQV) financed by national funds from FCT/MCTES (UIDB/50006/2020). N.G. acknowledges financial support from Fundação para a Ciência e a Tecnologia

(FCT) of Portugal (CEEC/2018). N.G. acknowledges support from UIDB/04046/2020 and UIDP/04046/2020 centre grants from FCT, Portugal (to BioISI).

REFERENCES

(1) Abbott, A. P.; Capper, G.; Davies, D. L.; Rasheed, R. K.; Tambyrajah, V. Novel solvent properties of choline chloride/urea mixturesElectronic supplementary information (ESI) available: spectroscopic data. See http://www.rsc.org/suppdata/cc/b2/b210714g/. *Chem. Commun.* **2003**, 70−71.

(2) Hansen, B. B.; Spittle, S.; Chen, B.; Poe, D.; Zhang, Y.; Klein, J. M.; Horton, A.; Adhikari, L.; Zelovich, T.; Doherty, B. W.; Gurkan, B.; Maginn, E. J.; Ragauskas, A.; Dadmun, M.; Zawodzinski, T. A.; Baker, G. A.; Tuckerman, M. E.; Savinell, R. F.; Sangoro, J. R. Deep Eutectic Solvents: A Review of Fundamentals and Applications. *Chem. Rev.* **2021**, *121*, 1232−1285.

(3) Smith, E. L.; Abbott, A. P.; Ryder, K. S. Deep Eutectic Solvents (DESs) and Their Applications. *Chem. Rev.* **2014**, *114*, 11060−11082.

(4) Clarke, C. J.; Tu, W.-C.; Levers, O.; Bröhl, A.; Hallett, J. P. Green and Sustainable Solvents in Chemical Processes. *Chem. Rev.* **2018**, *118*, 747−800.

(5) Li, X.; Row, K. H. Development of Deep Eutectic Solvents Applied in Extraction and Separation. *J. Sep. Sci.* **2016**, *39*, 3505−3520.

(6) Rente, D.; Paiva, A.; Duarte, A. R. The Role of Hydrogen Bond Donor on the Extraction of Phenolic Compounds from Natural Matrices Using Deep Eutectic Systems. *Molecules* **2021**, *26*, 2336.

(7) Pätzold, M.; Siebenhaller, S.; Kara, S.; Liese, A.; Syldatk, C.; Holtmann, D. Deep Eutectic Solvents as Efficient Solvents in Biocatalysis. *Trends Biotechnol.* **2019**, *37*, 943−959.

(8) Craveiro, R.; Meneses, L.; Durazzo, L.; Rocha, Â.; Silva, J. M.; Reis, R. L.; Barreiros, S.; Duarte, A. R. C.; Paiva, A. Deep Eutectic Solvents for Enzymatic Esterification of Racemic Menthol. *ACS Sustainable Chem. Eng.* **2019**, *7*, 19943−19950.

(9) Ma, C.; Sarmad, S.; Mikkola, J.-P.; Ji, X. Development of Low-Cost Deep Eutectic Solvents for CO 2 Capture. *Energy Procedia* **2017**, *142*, 3320−3325.

(10) Sarmad, S.; Mikkola, J.-P.; Ji, X. Carbon Dioxide Capture with Ionic Liquids and Deep Eutectic Solvents: A New Generation of Sorbents. *ChemSusChem* **2017**, *10*, 324−352.

(11) Paiva, A.; Craveiro, R.; Aroso, I.; Martins, M.; Reis, R. L.; Duarte, A. R. C. Natural Deep Eutectic Solvents - Solvents for the 21st Century. *ACS Sustainable Chem. Eng.* **2014**, *2*, 1063−1071.

(12) Santos, F.; Duarte, A. R. C. Therapeutic Deep Eutectic Systems for the Enhancement of Drug Bioavailability. In *Deep Eutectic Solvents for Medicine, Gas Solubilization and Extraction of Natural Substances*; Environmental Chemistry for a Sustainable World; Fourmentin, S., Costa Gomes, M., Lichtfouse, E., Eds.; Springer International Publishing: Cham, 2021; Vol. *56*, pp 103−129.

(13) Yadav, A.; Kar, J. R.; Verma, M.; Naqvi, S.; Pandey, S. Densities of aqueous mixtures of (choline chloride+ethylene glycol) and (choline chloride+malonic acid) deep eutectic solvents in temperature range 283.15-363.15K. *Thermochim. Acta* **2015**, *600*, 95−101.

(14) Hammond, O. S.; Bowron, D. T.; Edler, K. J. Liquid Structure of the Choline Chloride-Urea Deep Eutectic Solvent (Reline) from Neutron Diffraction and Atomistic Modelling. *Green Chem.* **2016**, *18*, 2736−2744.

(15) Aroso, I. M.; Paiva, A.; Reis, R. L.; Duarte, A. R. C. Natural deep eutectic solvents from choline chloride and betaine - Physicochemical properties. *J. Mol. Liq.* **2017**, *241*, 654−661.

(16) Mjalli, F. S.; Ahmed, O. U. Physical properties and intermolecular interaction of eutectic solvents binary mixtures: reline and ethaline. *Asia-Pac. J. Chem. Eng.* **2016**, *11*, 549−557.

(17) Abranches, D. O.; Silva, L. P.; Martins, M. A. R.; Pinho, S. P.; Coutinho, J. A. P. Understanding the Formation of Deep Eutectic Solvents: Betaine as a Universal Hydrogen Bond Acceptor. *ChemSusChem* **2020**, *13*, 4916−4921.

(18) Nowosielski, B.; Jamrógiewicz, M.; Łuczak, J.; Śmiechowski, M.; Warmińska, D. Experimental and Predicted Physicochemical Properties of Monopropanolamine-Based Deep Eutectic Solvents. *J. Mol. Liq.* **2020**, *309*, 113110.

(19) Harifi-Mood, A. R.; Buchner, R. Density, viscosity, and conductivity of choline chloride + ethylene glycol as a deep eutectic solvent and its binary mixtures with dimethyl sulfoxide. *J. Mol. Liq.* **2017**, *225*, 689−695.

(20) Agieienko, V.; Buchner, R. A Comprehensive Study of Density, Viscosity, and Electrical Conductivity of (Choline Chloride + Glycerol) Deep Eutectic Solvent and Its Mixtures with Dimethyl Sulfoxide. *J. Chem. Eng. Data* **2021**, *66*, 780−792.

(21) D'Agostino, C.; Harris, R. C.; Abbott, A. P.; Gladden, L. F.; Mantle, M. D. Molecular Motion and Ion Diffusion in Choline Chloride Based Deep Eutectic Solvents Studied by 1H Pulsed Field Gradient NMR Spectroscopy. *Phys. Chem. Chem. Phys.* **2011**, *13*, 21383.

(22) Zhu, S.; Li, H.; Zhu, W.; Jiang, W.; Wang, C.; Wu, P.; Zhang, Q.; Li, H. Vibrational Analysis and Formation Mechanism of Typical Deep Eutectic Solvents: An Experimental and Theoretical Study. *J. Mol. Graphics Modell.* **2016**, *68*, 158−175.

(23) Wagle, D. V.; Deakyne, C. A.; Baker, G. A. Quantum Chemical Insight into the Interactions and Thermodynamics Present in Choline Chloride Based Deep Eutectic Solvents. *J. Phys. Chem. B* **2016**, *120*, 6739−6746.

(24) Kovács, A.; Neyts, E. C.; Cornet, I.; Wijnants, M.; Billen, P. Modeling the Physicochemical Properties of Natural Deep Eutectic Solvents. *ChemSusChem* **2020**, *13*, 3789−3804.

(25) Atilhan, M.; Aparicio, S. Molecular Dynamics Simulations of Mixed Deep Eutectic Solvents and Their Interaction with Nanomaterials. *J. Mol. Liq.* **2019**, *283*, 147−154.

(26) Monteiro, H.; Santos, F.; Paiva, A.; Duarte, A. R. C.; Ferreira, R. J. Molecular Dynamics Studies of Therapeutic Liquid Mixtures and Their Binding to Mycobacteria. *Front. Pharmacol.* **2021**, *12*, 626735.

(27) Zhang, Y.; Poe, D.; Heroux, L.; Squire, H.; Doherty, B. W.; Long, Z.; Dadmun, M.; Gurkan, B.; Tuckerman, M. E.; Maginn, E. J. Liquid Structure and Transport Properties of the Deep Eutectic Solvent Ethaline. *J. Phys. Chem. B* **2020**, *124*, 5251−5264.

(28) Kaur, S.; Malik, A.; Kashyap, H. K. Anatomy of Microscopic Structure of Ethaline Deep Eutectic Solvent Decoded through Molecular Dynamics Simulations. *J. Phys. Chem. B* **2019**, *123*, 8291−8299.

(29) Contreras, R.; Lodeiro, L.; Rozas-Castro, N.; Ormazábal-Toledo, R. On the role of water in the hydrogen bond network in DESs: an ab initio molecular dynamics and quantum mechanical study on the urea-betaine system. *Phys. Chem. Chem. Phys.* **2021**, *23*, 1994−2004.

(30) Smith, P. J.; Arroyo, C. B.; Lopez Hernandez, F.; Goeltz, J. C. Ternary Deep Eutectic Solvent Behavior of Water and Urea-Choline Chloride Mixtures. *J. Phys. Chem. B* **2019**, *123*, 5302−5306.

(31) Ferreira, A. S. D.; Craveiro, R.; Duarte, A. R.; Barreiros, S.; Cabrita, E. J.; Paiva, A. Effect of Water on the Structure and Dynamics of Choline Chloride/Glycerol Eutectic Systems. *J. Mol. Liq.* **2021**, *342*, 117463.

(32) Roda, A.; Santos, F.; Chua, Y. Z.; Kumar, A.; Do, H. T.; Paiva, A.; Duarte, A. R. C.; Held, C. Unravelling the nature of citric acid:l-arginine:water mixtures: the bifunctional role of water. *Phys. Chem. Chem. Phys.* **2021**, *23*, 1706−1717.

(33) Hammond, O. S.; Bowron, D. T.; Edler, K. J. The Effect of Water upon Deep Eutectic Solvent Nanostructure: An Unusual Transition from Ionic Mixture to Aqueous Solution. *Angew. Chem.* **2017**, *129*, 9914−9917.

(34) Kaur, S.; Gupta, A.; Kashyap, H. K. How Hydration Affects the Microscopic Structural Morphology in a Deep Eutectic Solvent. *J. Phys. Chem. B* **2020**, *124*, 2230−2237.

(35) Rozas, S.; Benito, C.; Alcalde, R.; Atilhan, M.; Aparicio, S. Insights on the Water Effect on Deep Eutectic Solvents Properties and Structuring: The Archetypical Case of Choline Chloride + Ethylene Glycol. *J. Mol. Liq.* **2021**, *344*, 117717.

https://doi.org/10.1021/acssuschemeng.1c07461
ACS Sustainable Chem. Eng. 2022, 10, 3501−3512

(36) Passos, H.; Tavares, D. J. P.; Ferreira, A. M.; Freire, M. G.; Coutinho, J. A. P. Are Aqueous Biphasic Systems Composed of Deep Eutectic Solvents Ternary or Quaternary Systems? *ACS Sustainable Chem. Eng.* **2016**, *4*, 2881−2886.
(37) Shah, D.; Mjalli, F. S. Effect of Water on the Thermo-Physical Properties of Reline: An Experimental and Molecular Simulation Based Approach. *Phys. Chem. Chem. Phys.* **2014**, *16*, 23900−23907.
(38) Ma, C.; Laaksonen, A.; Liu, C.; Lu, X.; Ji, X. The Peculiar Effect of Water on Ionic Liquids and Deep Eutectic Solvents. *Chem. Soc. Rev.* **2018**, *47*, 8685−8720.
(39) Sapir, L.; Harries, D. Restructuring a Deep Eutectic Solvent by Water: The Nanostructure of Hydrated Choline Chloride/Urea. *J. Chem. Theory Comput.* **2020**, *16*, 3335−3342.
(40) Posada, E.; López-Salas, N.; Jiménez Riobóo, R. J.; Ferrer, M. L.; Gutiérrez, M. C.; del Monte, F. Reline Aqueous Solutions Behaving as Liquid Mixtures of H-Bonded Co-Solvents: Microphase Segregation and Formation of Co-Continuous Structures as Indicated by Brillouin and ^{1}H NMR Spectroscopies. *Phys. Chem. Chem. Phys.* **2017**, *19*, 17103−17110.
(41) El Achkar, T.; Fourmentin, S.; Greige-Gerges, H. Deep Eutectic Solvents: An Overview on Their Interactions with Water and Biochemical Compounds. *J. Mol. Liq.* **2019**, *288*, 111028.
(42) Baz, J.; Held, C.; Pleiss, J.; Hansen, N. Thermophysical properties of glyceline-water mixtures investigated by molecular modelling. *Phys. Chem. Chem. Phys.* **2019**, *21*, 6467−6476.
(43) López-Salas, N.; Vicent-Luna, J. M.; Imberti, S.; Posada, E.; Roldán, M. J.; Anta, J. A.; Balestra, S. R. G.; Madero Castro, R. M.; Calero, S.; Jiménez-Riobóo, R. J.; Gutiérrez, M. C.; Ferrer, M. L.; del Monte, F. Looking at the ″Water-in-Deep-Eutectic-Solvent″ System: A Dilution Range for High Performance Eutectics. *ACS Sustainable Chem. Eng.* **2019**, *7*, 17565−17573.
(44) Yang, B.; Zhang, Q.; Fei, Y.; Zhou, F.; Wang, P.; Deng, Y. Biodegradable Betaine-Based Aprotic Task-Specific Ionic Liquids and Their Application in Efficient SO_2 Absorption. *Green Chem.* **2015**, *17*, 3798−3805.
(45) Kaczmarek, D. K.; Gwiazdowska, D.; Juś, K.; Klejdysz, T.; Wojcieszak, M.; Materna, K.; Pernak, J. Glycine Betaine-Based Ionic Liquids and Their Influence on Bacteria, Fungi, Insects and Plants. *New J. Chem.* **2021**, *45*, 6344−6355.
(46) Rodrigues, L. A.; Cardeira, M.; Leonardo, I. C.; Gaspar, F. B.; Radojčić Redovniković, I.; Duarte, A. R. C.; Paiva, A.; Matias, A. A. Deep eutectic systems from betaine and polyols - Physicochemical and toxicological properties. *J. Mol. Liq.* **2021**, *335*, 116201.
(47) Zeng, C.-X.; Qi, S.-J.; Xin, R.-P.; Yang, B.; Wang, Y.-H. Synergistic behavior of betaine-urea mixture: Formation of deep eutectic solvent. *J. Mol. Liq.* **2016**, *219*, 74−78.
(48) Cardellini, F.; Tiecco, M.; Germani, R.; Cardinali, G.; Corte, L.; Roscini, L.; Spreti, N. Novel Zwitterionic Deep Eutectic Solvents from Trimethylglycine and Carboxylic Acids: Characterization of Their Properties and Their Toxicity. *RSC Adv.* **2014**, *4*, 55990−56002.
(49) Cook, R. L.; King, H. E.; Herbst, C. A.; Herschbach, D. R. Pressure and Temperature Dependent Viscosity of Two Glass Forming Liquids: Glycerol and Dibutyl Phthalate. *J. Chem. Phys.* **1994**, *100*, 5178−5189.
(50) Abbott, A. P.; Harris, R. C.; Ryder, K. S.; D'Agostino, C.; Gladden, L. F.; Mantle, M. D. Glycerol Eutectics as Sustainable Solvent Systems. *Green Chem.* **2011**, *13*, 82−90.
(51) Møller, C.; Plesset, M. S. Note on an Approximation Treatment for Many-Electron Systems. *Phys. Rev.* **1934**, *46*, 618−622.
(52) Dunning, T. H. Gaussian Basis Sets for Use in Correlated Molecular Calculations. I. The Atoms Boron through Neon and Hydrogen. *J. Chem. Phys.* **1989**, *90*, 1007−1023.
(53) Frisch, M. J.; et al. *Gaussian 09*, Revision D.01; Gaussian, Inc. 2013.: Wallingford CT, 2013.
(54) Van Der Spoel, D.; Lindahl, E.; Hess, B.; Groenhof, G.; Mark, A. E.; Berendsen, H. J. C. GROMACS: Fast, Flexible, and Free. *J. Comput. Chem.* **2005**, *26*, 1701−1718.
(55) Bussi, G.; Donadio, D.; Parrinello, M. Canonical Sampling through Velocity Rescaling. *J. Chem. Phys.* **2007**, *126*, 014101.
(56) Parrinello, M.; Rahman, A. Polymorphic Transitions in Single Crystals: A New Molecular Dynamics Method. *J. Appl. Phys.* **1981**, *52*, 7182−7190.
(57) Essmann, U.; Perera, L.; Berkowitz, M. L.; Darden, T.; Lee, H.; Pedersen, L. G. A Smooth Particle Mesh Ewald Method. *J. Chem. Phys.* **1995**, *103*, 8577−8593.
(58) Hess, B.; Bekker, H.; Berendsen, H. J. C.; Fraaije, J. G. E. M. LINCS: A Linear Constraint Solver for Molecular Simulations. *J. Comput. Chem.* **1997**, *18*, 1463−1472.
(59) Wang, J.; Wolf, R. M.; Caldwell, J. W.; Kollman, P. A.; Case, D. A. Development and Testing of a General Amber Force Field. *J. Comput. Chem.* **2004**, *25*, 1157−1174.
(60) Jorgensen, W. L.; Maxwell, D. S.; Tirado-Rives, J. Development and Testing of the OPLS All-Atom Force Field on Conformational Energetics and Properties of Organic Liquids. *J. Am. Chem. Soc.* **1996**, *118*, 11225−11236.
(61) Dodda, L. S.; Vilseck, J. Z.; Tirado-Rives, J.; Jorgensen, W. L. 1.14*CM1A-LBCC: Localized Bond-Charge Corrected CM1A Charges for Condensed-Phase Simulations. *J. Phys. Chem. B* **2017**, *121*, 3864−3870.
(62) Dodda, L. S.; Cabeza de Vaca, I.; Tirado-Rives, J.; Jorgensen, W. L. LigParGen Web Server: An Automatic OPLS-AA Parameter Generator for Organic Ligands. *Nucleic Acids Res.* **2017**, *45*, W331−W336.
(63) Cornell, W. D.; Cieplak, P.; Bayly, C. I.; Kollman, P. A. Application of RESP Charges to Calculate Conformational Energies, Hydrogen Bond Energies, and Free Energies of Solvation. *J. Am. Chem. Soc.* **1993**, *115*, 9620−9631.
(64) Abascal, J. L. F.; Vega, C. A General Purpose Model for the Condensed Phases of Water: TIP4P/2005. *J. Chem. Phys.* **2005**, *123*, 234505.
(65) Haile, J. M. *Molecular Dynamics Simulation: Elementary Methods*; Wiley Professional Paperback Series; Wiley: New York, 1997.
(66) Daivis, P. J.; Evans, D. J. Comparison of Constant Pressure and Constant Volume Nonequilibrium Simulations of Sheared Model Decane. *J. Chem. Phys.* **1994**, *100*, 541.
(67) Chen, T.; Smit, B.; Bell, A. T. Are Pressure Fluctuation-Based Equilibrium Methods Really Worse than Nonequilibrium Methods for Calculating Viscosities? *J. Chem. Phys.* **2009**, *131*, 246101.
(68) Segur, J. B.; Oberstar, H. E. Viscosity of Glycerol and Its Aqueous Solutions. *Ind. Eng. Chem.* **1951**, *43*, 2117−2120.
(69) Schröter, K.; Donth, E. Viscosity and Shear Response at the Dynamic Glass Transition of Glycerol. *J. Chem. Phys.* **2000**, *113*, 9101−9108.
(70) Yeh, I.-C.; Hummer, G. System-Size Dependence of Diffusion Coefficients and Viscosities from Molecular Dynamics Simulations with Periodic Boundary Conditions. *J. Phys. Chem. B* **2004**, *108*, 15873−15879.
(71) Moultos, O. A.; Zhang, Y.; Tsimpanogiannis, I. N.; Economou, I. G.; Maginn, E. J. System-Size Corrections for Self-Diffusion Coefficients Calculated from Molecular Dynamics Simulations: The Case of CO2, n-Alkanes, and Poly(Ethylene Glycol) Dimethyl Ethers. *J. Chem. Phys.* **2016**, *145*, 074109.
(72) Zichi, D. A.; Rossky, P. J. Solvent Molecular Dynamics in Regions of Hydrophobic Hydration. *J. Chem. Phys.* **1986**, *84*, 2814.
(73) Laage, D.; Stirnemann, G.; Hynes, J. T. Why Water Reorientation Slows without Iceberg Formation around Hydrophobic Solutes. *J. Phys. Chem. B* **2009**, *113*, 2428−2435.
(74) Galamba, N. Water Tetrahedrons, Hydrogen-Bond Dynamics, and the Orientational Mobility of Water around Hydrophobic Solutes. *J. Phys. Chem. B* **2014**, *118*, 4169−4176.
(75) Haselmeier, R.; Holz, M.; Marbach, W.; Weingaertner, H. Water Dynamics near a Dissolved Noble Gas. First Direct Experimental Evidence for a Retardation Effect. *J. Phys. Chem.* **1995**, *99*, 2243−2246.

https://doi.org/10.1021/acssuschemeng.1c07461
ACS Sustainable Chem. Eng. 2022, 10, 3501−3512

(76) Bakulin, A. A.; Pshenichnikov, M. S.; Bakker, H. J.; Petersen, C. Hydrophobic Molecules Slow Down the Hydrogen-Bond Dynamics of Water. *J. Phys. Chem. A* **2011**, *115*, 1821−1829.
(77) Abel, S.; Galamba, N.; Karakas, E.; Marchi, M.; Thompson, W. H.; Laage, D. On the Structural and Dynamical Properties of DOPC Reverse Micelles. *Langmuir* **2016**, *32*, 10610−10620.
(78) Martiniano, H. F. M. C.; Galamba, N. Fast and Slow Dynamics and the Local Structure of Liquid and Supercooled Water next to a Hydrophobic Amino Acid. *Phys. Chem. Chem. Phys.* **2016**, *18*, 27639−27647.
(79) Tomlinson, D. J. Temperature Dependent Self-Diffusion Coefficient Measurements of Glycerol by the Pulsed N.M.R. Technique. *Mol. Phys.* **1973**, *25*, 735−738.
(80) Kestin, J.; Sokolov, M.; Wakeham, W. A. Viscosity of liquid water in the range −8 °C to 150 °C. *J. Phys. Chem. Ref. Data* **1978**, *7*, 941.
(81) Mills, R. Self-Diffusion in Normal and Heavy Water in the Range 1-45.Deg. *J. Phys. Chem.* **1973**, *77*, 685−688.
(82) Shrake, A.; Rupley, J. A. Environment and Exposure to Solvent of Protein Atoms. Lysozyme and Insulin. *J. Mol. Biol.* **1973**, *79*, 351−371.
(83) Eisenhaber, F.; Lijnzaad, P.; Argos, P.; Sander, C.; Scharf, M. The Double Cubic Lattice Method: Efficient Approaches to Numerical Integration of Surface Area and Volume and to Dot Surface Contouring of Molecular Assemblies. *J. Comput. Chem.* **1995**, *16*, 273−284.
(84) Bondi, A. Van Der Waals Volumes and Radii. *J. Phys. Chem.* **1964**, *68*, 441−451.

https://doi.org/10.1021/acssuschemeng.1c07461
ACS Sustainable Chem. Eng. 2022, 10, 3501−3512